Acta metall. Vol. 35, No. 5, pp. 1067–1075, 1987
Printed in Great Britain.

0001-6160/87 $3.00 + 0.00

NUCLEATION OF GRAIN BOUNDARY CAVITIES UNDER THE COMBINED INFLUENCE OF HELIUM AND APPLIED STRESS

J. N. AL-HAJJI
Mechanical Engineering Department, University of Kuwait, Kuwait

and

N. M. GHONIEM
Mechanical, Aerospace and Nuclear Engineering Department, University of California, Los Angeles, CA 90024, U.S.A.

(*Received* 1 *January* 1986; *in revised form* 6 *August* 1986)

Abstract—Modelling cavity nucleation at grain boundaries in structural alloys under the combined influence of helium and stress is the primary objective of this paper. The role of stress in cavity nucleation is analyzed using an extension of classical theory by taking into account grain boundary sliding to describe stress concentration buildup and relaxation at particles and triple-point junctions. Helium clustering in the matrix is modeled using rate theory. The helium flux to grain boundaries is determined by the application of sink strength theory which takes into account the various competing clustering mechanisms in the matrix. Helium clustering on grain boundaries is also theoretically investigated using rate theory. The work agrees with experimental observations showing that irradiation results in grain boundary bubble densities which are orders of magnitude larger than cavity populations observed in conventional creep experiments. It is shown that even if the total injected helium is as little as one part per million, it can result in grain boundary bubble densities on the order of 10^{13} m^{-2}. Such cavity population exceeds typical grain boundary cavity densities associated with creep experiments. Grain boundary bubble densities are shown to reach steady state for injected helium amounts on the order of 10 parts per million.

Résumé—L'objectif principal de cet article est la modélisation de la germination intergranulaire des cavités dans des alliages de structure, sous l'influence combinée de l'hélium et d'une contrainte. Nous analysons le rôle de la contrainte dans la germination des cavités en utilisant une extension de la théorie classique de la germination, et en tenant compte du glissement intergranulaire pour décrire la création et la relaxation d'une accumulation de contrainte au niveau des particules et des jonctions triples. Nous modélisons la création d'amas d'hélium à l'aide d'une théorie d'activation. Nous déterminons le flux d'hélium vers les joints de grains en appliquant une théorie de force de piégeage qui tient compte des différents mécanismes de piégeage en compétition dans la matrice. Nous étudions aussi théoriquement la ségrégation intergranulaire de l'hélium en utilisant une théorie d'activation. Ces études concordent avec les observations expérimentales qui montrent que l'irradiation produit des densités de bulles intergranulaires de plusieurs ordres de grandeur supérieures à celles des cavités que l'on observe dans les expériences classiques de fluage. Nous montrons que même si la quantité totale d'hélium injecté est aussi faible que 10^{-6}, les densités intergranulaires de bulles peuvent être de l'ordre de 10^{13} m^{-2}. Une telle population de cavités dépasse les densités typiques de cavités intergranulaires associées aux expériences de fluage. Nous montrons que les densités de bulles intergranulaires atteignent un état d'équilibre pour des quantités d'hélium injecté de l'ordre de 10^{-5}.

Zusammenfassung—Die Modellbeschreibung der Bildung von Hohlräumen an Korngrenzen unter dem gemeinsamen Einfluß von Helium und Spannung wird in dieser Arbeit behandelt. Der Rolle der Spannung bei der Hohlraumbildung wird mit einer Erweiterung der klassischen Keimbildungstheorie analysiert. Hierbei wird die Korngrenzgleitung zur Beschreibung des Aufbaus von Spannungskonzentrationen und der Relaxation an Teilchen und Dreierknoten berücksicht. Die Ansammlung von Helium in der Matrix wird mit der Ratentheorie modelliert Der Heliumfluß zur Korngrenze wird mit der Theorie der Senkenstärke bestimmt, die die verschiedenen konkurrierenden Ansammlungsmechanismen in der Matrix berücksichtigt. Die Ansammlung des Heliums an der Korngrenze wird mit der Ratentheorie theoretisch auch untersucht. Die Arbeit stimmt mit experimentellen Untersuchunge überein, die zeigen, daß Bestrahlung zu Blasendichtan an den Korngrenzen führt, die Größenordnungen über den nach herkömmlichen Kriechexperimenten beobachteten liegen. Es wird gezeigt, daß sogar bei einer Gesamtkonzentration an Helium von nur ein ppm Blasendichten von der Ordnung 10^{13} m^{-2} an den Korngrenzen auftreten können. Eine solche Dichte ist schon höher als die typischen Dichten, die nach Kriechexperimenten an den Korngrenzen beobachtet werden. Es wird gezeigt, daß die Dichte der Blasen an den Konrgrenzen für eine Größenordnung von 10 ppm an eingebrachtem Helium einen stationären Wert erreicht.

1. INTRODUCTION

Over the past decade, a number of theoretical and experimental investigations have addressed the question of cavity nucleation at grain boundaries [1–10]. For example, Raj and Ashby [4] developed a kinetic model of classical heterogeneous nucleation by vacancy clustering at interfaces between precipitate particles and grain boundaries. Their work revealed that cavity nucleation is in fact stress controlled. However, under irradiation at high temperatures, it has been observed [10–15] that the population of cavities at grain boundaries is typically 4–5 orders of magnitude higher than unirradiated creep-tested specimens. This has been attributed to the presence of helium at such boundaries. The distinction between cavity nucleation by helium versus stress has to be made.

In the present paper, theoretical investigation of cavity nucleation at the grain boundary under the influence of stress and helium is given. The stress-controlled mode of cavity nucleation is analyzed using an extension to classical nucleation theory by taking into account the role of sliding in generating highly localized stress concentrations at boundary irregularities and triple-point junctions. The helium-controlled mode of cavity nucleation is modeled via rate theory to describe the clustering of helium atoms at grain boundaries into stable nuclei. The objective of this paper is to investigate the relative importance of applied stress and helium generation during irradiation on grain boundary cavity nucleation. The modes and mechanisms of cavity nucleation are analyzed using a self-consistent time-dependent model.

2. STRESS-CONTROLLED NUCLEATION OF CAVITIES

At elevated temperatures of $\sim 0.6\,T_m$ and medium applied stresses of $\sim 10^{-3}\,G$ (G is the shear modulus), grain boundary cavities are nucleated by diffusional transfer of atoms from grain boundary precipitate surfaces into the grain boundary. This results in the formation of a vacancy cluster which is large enough to overcome the shrinkage tendency under the action of surface energy forces. The local tensile traction plays a considerable role in aiding cavity embryos to grow through a size range where growth is energetically unstable.

Application of classical nucleation theory shows that the nucleation rate $\dot{C}$ (the product of the number of nuclei at the critical size, the probability that a vacancy will be added to a critical nucleus, and the Zeldovich factor which takes into account thermal fluctuations between the subcritical and supercritical regimes) is given by [16].

$$\dot{C} = C_{max}\left(\frac{\pi}{3F_v\gamma_s^3 kT}\right)^{1/2} \tfrac{1}{2}\sigma_L^2 D_{gb}\Delta \exp\left(-\frac{\Delta G_c}{kT}\right). \quad (1)$$

ΔG_c is the change in the free energy due to the introduction of cavities on a stressed boundary and it is given by

$$\Delta G_c = 4\gamma_s^3 F_v/\sigma_L^2 \quad (2)$$

or

$$\Delta G_c = r_c^3 F_v \sigma_L/2 \quad (3)$$

where $r_c = 2\gamma_s/\sigma_L$. Equation (1) does not account for the fact that once a cavity is nucleated, its site is no longer available for any additional nucleation. An additional probabilistic factor needs to be included to account for the decreasing number of available nucleation sites. This is given by

$$P_s = \frac{C_{max} - C}{C_{max}}. \quad (4)$$

Including equation (4) into equation (1) gives

$$\dot{C} = (C_{max} - C) \times \left(\frac{\pi}{12F_v\gamma_s^3 kT}\right)^{1/2} \sigma_L^2 D_{gb}\Delta \exp\left(-\frac{\Delta G_c}{kT}\right). \quad (5)$$

If we denote all terms within the large brackets by $A(t)$, then we can rewrite equations (5) as

$$\frac{dC}{dt} = (C_{max} - C)A(t). \quad (6)$$

The term $A(t)$ is strongly time dependent since the local stress is a complex function of time as it is influenced by the diffusional flow of matter. Equation (6) is subject to the initial condition: $C(0) = 0$.

Inspecting equation (5), we notice two values which have been the center of controversy: σ_L and F_v. Typical stresses necessary for nucleation are found to be about 30 times greater than applied stresses [17]. However, such high stress concentrations may be reached due to the instantaneous stress relaxation by diffusional flow of matter [1]. It has also been argued [1, 4] that cavities assume thin, crack-type shapes.

Examining the behavior of ΔG_c for a shape factor of 0.01 and a typical surface energy of 2 J/m^2 shows that even in the presence of a relatively high local stress, the barrier to nucleation is high (22.13 eV for an applied stress of 300 MPa). Equations (2) and (3) indicate that there are two possible ways to reduce the energy barrier to nucleation: (1) the cavities must be extremely thin (reducing F_v), and/or (2) the local stress has to reach extremely high values. It can be shown that if the local stress is 100 MPa, the shape factor should be in the neighborhood of 10^{-4}; otherwise nucleation will be impossible. Such extreme values of F_v have been suggested by Reidel [1] and Raj and Ashby [4]. The other possibility is that stress concentrations have to be present at inclusions and triple points in order for cavity nucleation to proceed [8, 10, 18]. The critical free energy for cavity formation varies significantly as a function of the local stress ($\Delta G_c \sim \sigma_L^{-2}$). It is concluded that a stress concentration mechanism has to be present in order to make nucleation possible. The shape factor value of about 0.01 has been adopted as reasonable by many

investigators [4, 19]. However, other investigators [20] asserted that F_v has a value of ~ 0.3 according to their experimental observations, which indicates an uncertainty in the actual value of F_v.

2.1. Stress concentration at particles and triple-point junctions

At high temperatures, the shearing resistance of grain boundaries is apparently less than the shearing resistance of individual grains themselves (e.g. Ref. [21]). However, if particles are present at sliding grain boundaries, stress concentrations approaching the ideal cohesive strength limit will be present at particle faces, as shown by Lau [22] and also by Reidel [1]. This can be readily seen by a simple force balance of a particle on a sliding boundary. Let us denote the particle spacing as L and its diameter as P located on a boundary. A shear stress τ will then give a localized particle facial stress of $\sigma_P = \tau(L/P)^2$. Such a particle stress is quite substantial and can explain the fact that obstacles at sliding boundaries are preferential sites for cavity nucleation. Reidel's calculations [1] show that in the absence of any diffusional flow, the average stress on the particle is on the order of $\sigma_P \simeq \tau(L/P)^2$.

Lau [22] made calculations of the stress-concentration factors associated with grain boundary inclusions and triple-point junctions in a power-law creeping material using the finite element technique. His work shows that a singularity develops at the triple-point junction (Fig. 1) which is of the form

$$\sigma_{\theta\theta} = K_{TPJ}/x^{\lambda_{TPJ}}. \tag{7}$$

For a creep exponent of $m = 1$, it is shown [22] that

$$\sigma_{\theta\theta}/\sigma_\infty = 0.3(d/x)^{0.449}. \tag{8}$$

We use Lau's Solution [22] of the stress distribution around triple-point junctions, which shows resemblance to the solution of the tensile-stress concentration of a single-mode-II penny-shaped crack loaded by the shear stress $\sigma_\infty/2$. The penny-shaped-crack problem has been adopted by Evans *et al.* [5] to study the time-dependent behavior of the stress singularity at triple-point junctions.

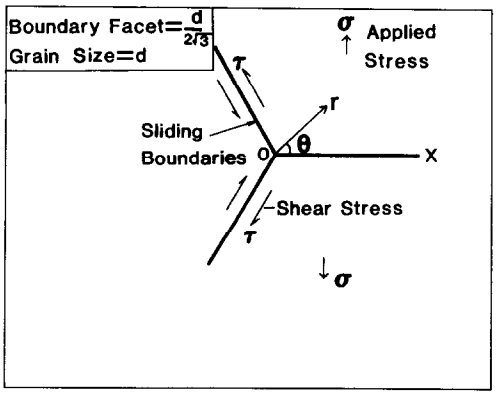

Fig. 1. Idealization of a triple-point junction.

2.2. Stress buildup and relaxation at particles

The simplest description of stress loading and unloading is provided by a phenomenological visco-elastic model which yields an expression given by [23, 24]

$$\sigma_p(t) = (\tau_0 - \tau^*)\exp(-t/\tau_L) + (\tau^* - \tau_\infty)\exp(-t/\tau_R) + \tau_\infty \tag{9}$$

where τ_L and τ_R represent the loading and relaxation times, respectively. For all practical purposes

$$\tau_\infty = \tau_0 = \sigma_{applied}/2 \tag{10}$$

and

$$\tau^* = \tau_0/f \tag{11}$$

where

$$f = (P/L)^2. \tag{12}$$

f is the fractional area of the boundary occupied by particles; τ_R, which is volume/grain boundary diffusion controlled, is the shortest relaxation time for smoothing out the singularity.

The characteristic time for stress loading at particles is given as [6]

$$\tau_{BR} = \tau_L = \frac{\eta L}{\pi G \Delta}\beta(P/L) \tag{13}$$

where η is the boundary viscosity which is given by Ashby [25] as

$$\eta = \frac{kT}{8\Delta D_{gb}} \tag{14}$$

and

$$\beta(P/L) = \cosh^{-1}\{1/[\cos(\pi/2)](1 - P/L)\}. \tag{15}$$

β accounts for the interactions of inter-particle planar segments on the grain boundary.

The characteristic time for boundary diffusional relaxation of the stress concentration at particles is given by Koeller and Raj [26]. For very rigid particles the relaxation time is given by

$$\tau_{R,BDIFF} \simeq \frac{L^3 kT}{G\Delta D_{gb}\Omega}. \tag{16}$$

Now if we use the usual criteria for a changeover from boundary to volume diffusion ($D_{gb}\ \Delta \rightarrow L D_v$) [27], we obtain

$$\tau_{R,VDIFF} \simeq \frac{L^2 kT}{G D_v \Omega}. \tag{17}$$

2.3. Stress loading and relaxation at grain boundary particles and triple-point junctions

When a stress is suddenly applied to polycrystalline solids at elevated temperature, instantaneous homogenous elastic deformation sets in. The resolved shear stress at the grain boundary interfaces are relaxed by sliding which results in stress concentrations at grain boundary irregularities such as interface particles. However, diffusional transfer of matter from these

sites leads to relaxation of the high localized stress. This results in a gradual buildup of a stress concentration at irregularities of a larger spatial scale (i.e. a gradual buildup of stress concentration at triple-point junctions). The Evans *et al.* solution [5] of the time-dependent behavior of the stress singularity at triple-point junctions yields

$$\sigma(0,t) = \tfrac{1}{9}\sigma_\infty (\tau_R^{TPJ}/t)^{1/6} \tag{18}$$

where

$$\tau_R^{TPJ} = \frac{(1-\nu)kTd^3}{GD_{gd}\Delta\Omega} \tag{19}$$

is a characteristic stress relaxation time constant. Equation (18) describes the stress relaxation in the vicinity of triple-point junctions. However, this expression does not take into account any loading time. Following Yoo and Trinkaus [16], a characteristic exponential loading time can be introduced into the Evans *et al.* model to describe the overall time behavior of the stress at triple-point junctions. The following expression results for the normal stress at the intersection.

$$\sigma_{TPJ} = \sigma_\infty \left\{ 1 + \frac{1}{9}\left[1 - \exp\left(-\frac{t}{\tau_L^{TPJ}} \right) \right] \left(\frac{\tau_R^{TPJ}}{t} \right)^{1/6} \right\}. \tag{20}$$

In this expression, τ_L^{TPJ} represents a characteristic loading time of stress at triple-point junctions and is determined by the overall intrinsic viscosity of the boundary, including the effect of particles at the boundary [24]

$$\tau_L^{TPJ} = \frac{d}{50G}\frac{kT}{\Omega}\frac{P^4}{L^2}\frac{1}{\Delta D_{gb}}. \tag{21}$$

In this section, we have extended classical nucleation theory to study the time-dependent nucleation of stress-induced cavities. A large number of vacancies is required to constitute the critical cavity nucleus size, making the application of a dynamic rate theory impractical. Classical nucleation theory is therefore a convenient approach, even though uncertainties still exist in some of its ingredients. On the other hand, for gas-containing cavities, we will use tri-atomic nucleation. Helium-vacancy binding energies are large, such that only two to three helium atoms are required for the stabilization of the critical nucleus [28]. In the next section, we present a dynamic rate-theory model for helium-assisted cavity nucleation at grain boundaries. A small number of rate equations are required to describe cavity nucleation, since the critical size contains only three helium atoms.

3. HELIUM TRANSPORT AND CLUSTERING AT GRAIN BOUNDARIES

There is a great tendency for helium atoms to be trapped on vacancies, impurity atoms, or other helium atoms [28–40]. The transport of helium to grain boundaries is primarily by migration of single gas atoms through the matrix [28] which is naturally influenced by competing clustering processes. Helium atoms, which migrate predominantly by an interstitial mechanism, can be trapped at precipitate interfaces, vacancies, or in helium-vacancy clusters (HVCs). A rate theory model has been developed to study helium migration from the matrix to the grain boundary. While details of the model have been published elsewhere [41], a brief summary will be presented here for the sake of self-consistency.

In this matrix transport/clustering model [41], appropriate rate equations were given for the following species: (1) unoccupied vacancies, (2) self-interstitial atoms, (3) interstitial helium atoms, (4) substitutional helium atoms, (5) di-interstitial helium atom clusters, (6) di-helium single-vacancy clusters, (7) bubble nuclei containing three helium atoms, and (8) large bubbles containing m helium atoms. Equations for the average bubble size, the average number of helium atoms in a bubble, and the amount of helium absorbed on grain boundaries were also developed. It is also assumed that one helium bubble is associated with each precipitate. Therefore, an equation describing the average precipitate bubble radius and another equation for the average number of helium atoms in a bubble were included. A key equation was developed to account for single interstitial helium atoms escaping the competing matrix processes until trapped at the grain boundary.

Helium production at the grain boundary is primarily due to single interstitial helium atoms escaping the interior grain traps. Since interior grain traps change with irradiation, the production of helium at the grain boundary is time dependent. Vacancies at grain boundaries are assumed to be readily available to trap helium interstitials. Once a tri-helium cluster is formed with some vacancies, a bubble embryo is assumed to be nucleated.

Four equations are developed here for concentration of the following species: (1) single helium atoms, C_g^{gb}, (2) di-helium atomic clusters, C_{2g}^{gb}, and (3) large bubbles containing m helium atoms, C_b^{gb}. An equation that describes the average number of helium atoms in a bubble, m_b^{gb}, is also presented.

$$\frac{dC_g^{gb}}{dt} = Q_{gb} - 2R_{g,g}^{gb} C_g^{gb2} - R_{g,2g}^{gb} C_g^{gb} C_{2g}^{gb} - R_{g,b}^{gb} C_g^{gb} C_b^{gb} - bKC_g^{gb} - R_{g,bppt}^{gb} C_g^{gb} C_{bppt}^{gb}, \tag{22}$$

$$\frac{dC_{2g}^{gb}}{dt} = R_{g,g}^{gb} C_g^{gb2} - 2bKC_{2g}^{gb} - R_{g,2g}^{gb} C_g^{gb} C_{2g}^{gb}, \tag{23}$$

$$\frac{dC_b^{gb}}{dt} = \frac{3}{m_b^{gb}} R_{g,2g}^{gb} C_g^{gb} C_{2g}^{gb}, \tag{24}$$

$$\frac{dm_b^{gb}}{dt} = R_{g,b}^{gb} K_g^{gb} - bKm_g^{gb}. \tag{25}$$

Now define the helium atom impingement frequency as

$$\alpha = 48\, \nu_g \exp\left(-\frac{E_{He}^{GB}}{kT} \right), \quad s^{-1}. \tag{26}$$

The combinatorial factor for bubbles at the grain boundary can easily be shown to be given by

$$\epsilon = \frac{4\pi}{48}\left(\frac{R}{a}\right). \tag{27}$$

With the reaction frequency α and the combinatorial number ϵ, the gas reaction rates at grain boundaries are given by

$$R^{gb}_{g,g} \simeq R^{gb}_{g,2g} \simeq 2\alpha, \quad R^{gb}_{g,b} \simeq \epsilon\alpha. \tag{28}$$

The superscript, gb, may now be removed from the equations for simplicity, and the previous set of equations can be re-written in the following form:

$$\frac{dC_g}{dt} = Q_{gb} - 4\alpha C_g^2 - 4\alpha C_g C_{2g} - \epsilon\alpha C_g C_b - \epsilon^{ppt}\alpha C_g C_{bppt} - bKC_g, \tag{29}$$

$$\frac{dC_{2g}}{dt} = 2\alpha C_g^2 - 2\alpha C_g C_{2g} - 2bKC_g, \tag{30}$$

$$\frac{dC_b}{dt} = \frac{6\alpha}{m_b} C_g C_{2g}, \tag{31}$$

$$\frac{dm_b}{dt} = \epsilon\alpha C_g - bKm_b. \tag{32}$$

Equation (29) represents the rate of change of single-helium atom concentration at grain boundaries, C_g. The source of helium, Q_{gb}, which is supplied by helium transport through the matrix, is balanced by the formation of helium clusters, by absorption at newly formed bubbles, by precipitates, or by radiation re-solution back into the matrix. Equation (30) describes the rate of change of di-helium clusters, while equation (31) is for the nucleation rate of helium-filled cavities at grain boundaries. Equation (32) determines the rate of change of the average number of helium atoms in a cavity m_b due to the balance between the absorption rate, $\epsilon\alpha C_g$, and radiation re-solution rate, bKm_b. Obviously, this set of equations has to be solved self-consistently with the corresponding set representing matrix processes [41], the coupling rate being Q_{gb}.

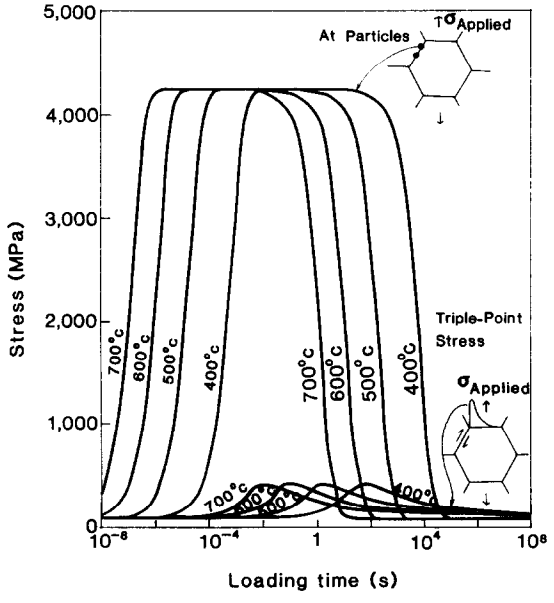

Fig. 2. Stress loading and relaxation at particles and triple-point junctions for an applied stress of 100 MPa, a grain size of 50 μm, a particle size of 0.03 μm, and spacing of 0.21 μm. (Material parameters are for 304 stainless steel.)

4. RESULTS

Figure 2 shows that the overall time dependence of stress evolution at triple-point junctions is much slower than that at particle interfaces. This is because the time dependence of the stress concentration at triple-point junctions is characterized by a wide spectrum of relaxation times, i.e. short relaxation times controlling the early stages and long ones controlling the later stages [5]. This is in contrast with stress relaxation times at particles in which diffusional matter flow needs only to occur over short distances in order to relieve the stress. This figure also shows that the duration of the stress pulse becomes quite short at higher temperatures. At lower temperatures, the triple-point junction stress becomes quite persistent for a reasonably long time. This may explain observed triple-point cracking at temperatures below about 400°C [42], since persistent stress concentration at triple-point junctions leads to crack initiation. Stress pulses shown in Fig. 2 are used later in nucleation calculations.

It is also shown on Fig. 2 that, at low temperatures ($\lesssim$ 400°C), the triple-point stress concentration prevails for a long period of time and can result in the opening of a crack at the triple point by decohesion. One concludes that triple-point cracking can be due to decohesion at lower temperatures; but at higher temperatures, cavitation near the triple point plays a major role in opening such a crack.

It has been experimentally observed (e.g. [7]) that high temperature fracture occurs due to the nucleation and growth of cavities along grain boundaries which are mostly perpendicular to the applied stress. However, two experimental studies directed toward understanding cavity nucleation at high temperatures (Dyson *et al.* [43], and Kikuchi *et al.* [44]) showed that most nucleated cavities have formed on grain boundaries which are parallel to the maximum principal stress axis. The experiment by Dyson *et al.* [43] also showed that preferential cavity growth occurred during subsequent tensile creep. Those cavities on parallel boundaries either remained constant in size or diminished, while those on boundaries which were orthogonal to the applied stress axis grew relatively quickly.

In order to model nucleation at orthogonal boundaries which exhibit localized irregularities [45, 46], we assume here that a boundary exhibits localized sliding because of deviations from orthogonality by about

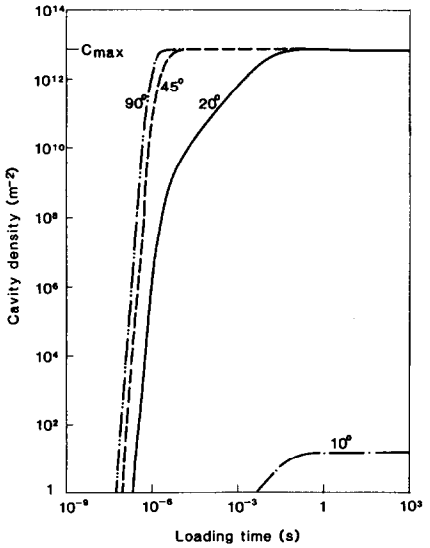

Fig. 3. Density of cavity nuclei at boundaries of various inclinations at 600°C and $F_v = 0.01$ as a result of a single sliding pulse. The applied stress is 100 MPa. (Material parameters are for 304 stainless steel.)

10–20 deg. Figure 3 shows that the nucleation rate is the highest along boundaries which are parallel to the applied stress and decreases sharply as boundaries tend toward orthogonality. At orthogonal flat boundaries, nucleation is essentially non-existent. The nucleation pulse closely follows the stress pulse behavior; the nucleation pulse is terminated once the stress pulse has elapsed. At 600°C, the nucleation pulse lasts ~ 100 s. If the nucleation rate is high, all possible nucleation sites will be filled up by cavities. If the nucleation rate is low, cavity nucleation will occur throughout the creep experiment following the course of stress concentration buildup and relaxation in response to localised sliding which should occur intermittently.

Figure 4 shows that the nucleation rate is the highest at 700°C and decreases as the temperature decreases. More extensive nucleation occurs at higher temperatures, which is consistent with experimental observations presented by Argon *et al.* [6]. The figure also shows another important result: the duration of the nucleation pulse is sharply curtailed at high temperatures. The basic reason for this behavior is that stress relaxation is faster at high temperatures because of the higher atomic diffusion rates. At lower temperatures, the duration of the stress pulse is long, but the nucleation rate is too low to result in significant cavitation.

Experimental observations by Chen and Argon [7] show that more extensive nucleation occurs near triple-point junctions. As was shown in the previous section, high stress concentrations exist at triple-point junctions and prevail for a relatively long period of time. This stress results in an enhanced sliding rate past grain boundary irregularities and in high stress concentrations at neighboring particles. The relaxation of the triple-point stress concentration is quite slow and can be attributed to the large distance over which uniform atom plating has to occur.

The rate of clustering of helium at grain boundaries is influenced mainly by the effective migration energy of single helium atoms. The effective migration energy of helium in the matrix has been studied in detail by Ghoniem *et al.* [28]; very little is known, however, about its value at grain boundaries.

It is generally believed that helium atoms introduced at grain boundaries reside in a substitutional position since the supply of vacancies at grain boundaries is nearly inexhaustible. Figure 5 shows the sensitivity of the grain boundary bubble density to the effective helium migration energy. The irradiation

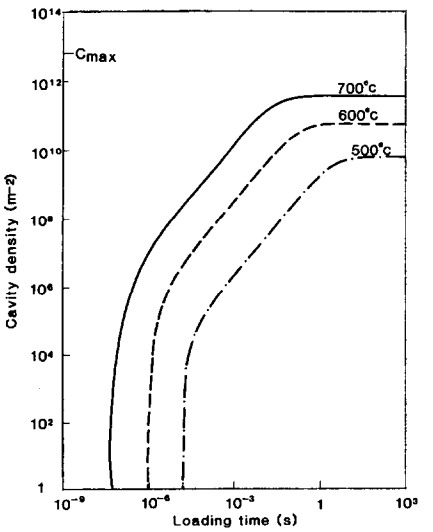

Fig. 4. Density of cavity nuclei as a function of temperature for $F_v = 0.01$, a boundary inclination of 15 deg, and an applied stress of 100 MPa. (Material parameters are for 304 stainless steel.)

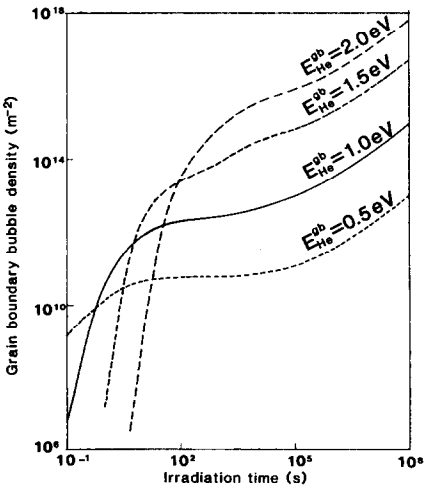

Fig. 5. The effect of the grain boundary migration energy on the grain boundary bubble density for 316 stainless steel under dual ion-beam irradiation at 625°C. The displacement rate is 3×10^{-3} dpa/s and the He/dpa ratio is 5 (appm/dpa).

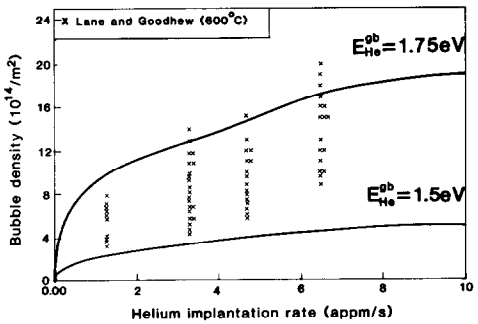

Fig. 6. The influence of the He migration energy on the grain boundary bubble density of the ternary austenitic alloy Fe–15%Cr–15%Ni. The total injected He is 5600 appm and the He/dpa ratio is 1.6×10^4 appm/dpa. (Data from Ref. [15].)

conditions simulated in the figure are that of dual ion-beam irradiation which are conducted at 625°C on type 316 stainless steel. The displacement rate is 3×10^{-3} dpa/s and the helium to dpa ratio is 5 (appm/dpa). Increasing the effective migration energy results in enhanced nucleation. A migration energy of 1.5–2.0 eV results in a bubble density consistent with those observed experimentally [11–15].

Figure 6 is a comparison between our theoretical calculations and the experimental data of Lane and Goodhew [15] on grain boundary bubble nucleation in the ternary austenitic alloy, Fe–15%Cr–15%Ni. The figure shows the bubble density as a function of the helium implantation rate. The experiments were carried out at 600°C with a helium to dpa ratio of 1.6×10^4 (appm/dpa). It is clearly demonstrated that the bubble density increases with an increasing implantation rate. The model successfully shows the correct trends as compared to experiments. The figure also illustrates that increasing the grain boundary helium migration energy enhances bubble nucleation.

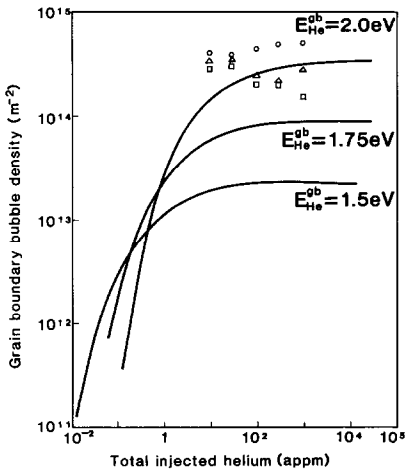

Fig. 7. Grain boundary bubble density as a function of the He concentration for AISI 316 stainless steel. The helium dpa ratio is 10^4 (appm/dpa) and the implantation rate is 100 appm/h at 750°C. (Data from Ref. [12].)

Figure 7 shows a comparison between the present theory and the grain boundary bubble nucleation experiments conducted by Batfalsky and Schroeder [12] on AISI 316 stainless steel. The helium to dpa ratio is 10^4 (appm/dpa). The helium implantation rate is 100 appm/h at 750°C. The simulation shows that the effective migration energy is approximately the same as that for self-diffusion. A self-diffusion energy of 1.9 eV has been reported by Smith and Gibbs [47]. The figure also shows that the helium clustering rate is extremely high during early irradiation and that it slows down as the amount of helium arriving at the grain boundary is in equilibrium with radiation resolution.

5. CONCLUSIONS

A time-dependent extension to classical nucleation theory has shown that, in the absence of irradiation, grain boundary sliding is the driving force for grain boundary cavity nucleation. When sliding is resisted by triple-point junctions or by hard particles at grain interfaces, sufficiently high localized stresses are set up and immediately relaxed by diffusion or dislocation creep. The ensuing nucleation pulse is shown to be sensitive to the cavity shape and to the boundary inclination to the applied stress. Stress-induced cavity nucleation can therefore be statistical and dependent on the stochastic nature of sliding, and the distribution of irregularities on boundaries normal to the applied stress. It is concluded that, with a cavity shape factor on the order of 0.01 and surface normal inclinations of only 15–20 deg to the applied stress, a small number of such nucleation pulses is required to saturate all available nucleation sites. It is also shown that stress-induced cavity nucleation is very rapid and that cavity life is spent mainly in the growth regime.

Under irradiation, the introduction of helium via nuclear reactions results in a dynamic helium flux to grain boundaries. This atomic helium flux drives another mode of grain boundary cavity nucleation by helium-vacancy clustering. The rate theory of helium clustering presented here shows that this mode of cavity nucleation is much stronger than the stress-induced mode. With a total helium as little as 1 appm, helium-nucleated grain boundary cavity densities on the order of 10^{13} m^{-2} may result. The present work and experiments on grain boundary cavitation by helium are in basic agreement. The effective helium migration energy on the grain boundary for such an agreement is on the order of the self-diffusion energy. Calculated grain boundary bubble densities in the presence of irradiation are several orders of magnitude greater than cavity densities in the absence of irradiation. These quasi-steady-state densities are reached rather quickly at helium contents on the order of 10 appm. The model also shows that, consistent with experiments, the saturation cavity density increases with increasing helium implantation rate.

However, the dependence of cavity density on the helium implantation rate is sub-linear.

Acknowledgements—This work is partially supported by the U.S. Department of Energy, Grant No. DE-FG03-84ER52110 with UCLA. One of us (J.N.A.) is grateful to Kuwait University for financial support during his graduate study at UCLA.

REFERENCES

1. H. Reidel, *Acta metall.* **32,** 313 (1984).
2. A. S. Argon, *Scripta metall.* **17,** 5 (1983).
3. R. Raj, *Acta metall.* **26,** 995 (1978).
4. R. Raj and M. F. Ashby, *Acta metall.* **23,** 653 (1975).
5. A. G. Evans, J. R. Rice and J. P. Hirth, *J. Am. Ceram. Soc.* **63,** 368 (1980).
6. A. S. Argon, I. W. Chen and C. W. Lau, in *Creep-Fatigue-Environment Interactions* (edited by R. M. Pelloux and N. S. Stoloff), p. 46. A.I.M.E., New York (1980).
7. I. W. Chen and A. S. Argon, *Acta metall.* **29,** 1321 (1981).
8. W. Pavinich and R. Raj, *Metall. Trans. A* **8A,** 1917 (1977).
9. I. Servi and N. J. Grant, *Trans. Am. Inst. Min. Engrs* **191,** 909 (1951).
10. J. E. Harris, *Trans. metall. Soc. A.I.M.E.* **233,** 1509 (1965).
11. A. F. Rowcliffe, G. J. C. Carpenter, H. F. Merrick and R. B. Nicholson, *Effects of Radiation on Structural Metals*, ASTM STP-426, pp. 161–199. A.S.T.M. (1967).
12. P. Batfalsky and H. Schroeder, *J. Nucl. Mater.* **122 & 123,** 1475 (1984).
13. J. I. Bennetch and W. A. Jesser, *J. Nucl. Mater.* **103 & 104,** 809 (1981).
14. P. L. Lane, J. H. Evans and P. J. Goodhew, *J. Nucl. Mater.* **120,** 342 (1984).
15. P. L. Lane and P. J. Goodhew, *Phil. Mag.* (A) **48,** 965 (1983).
16. M. H. Yoo and H. Trinkaus, *Metall. Trans. A* **14A,** 547 (1983).
17. A. S. Argon, *Recent Advances in Creep and Fracture of Engineering Materials and Structures* (edited by B. Wilshire and D. R. J. Owen), pp. 1–52. Pineridge Press, Swansea (1982).
18. F. W. Crossman and M. F. Ashby, *ibid.*, Ref. [4], p. 425.
19. H. Trinkaus and H. Ullmaier, *Phil. Mag.* **39,** 563 (1979).
20. A. L. Chang and M. L. Bleiberg, Ward Topical Report WARD-AD-3045-12, 259 (1980).
21. C. Zener, Presented at: *Fracturing of Metals Seminar*, American Society for Metals, Chicago p.3 (1948).
22. C. W. Lau, Ph.D. thesis, Massachusetts Institute of Technology (1981).
23. H. Trinkaus, *Phil. Mag.* In press.
24. J. N. Al-Hajji, Ph.D. thesis, Univ. of California, Los Angeles (1985); also UCLA report UCLA-ENG-8533/PPG-894 (1985).
25. M. F. Ashby, *Surf. Sci.* **31,** 498 (1972).
26. R. C. Koeller and R. Raj, *ibid.*, Ref. [3], p. 1551.
27. R. Raj and M. F. Ashby, *Metall. Trans. A* **2A,** 1113 (1971).
28. N. M. Ghoniem, S. Sharafat, J. M. Williams and L. K. Mansur, *J. Nucl. Mater.* **117,** 96 (1983).
29. M. I. Baskes, C. L. Bisson and W. D. Wilson, *J. Nucl. Mater.* **83,** 139 (1979).
30. G. Carter, D. G. Armour, S. E. Donnelly, D. C. Ingram and R. P. Webb, Presented at: *Harwell Consultants Symposium*, Oxfordshire, England, p. 83 (1979).
31. G. Farrell and W. A. Grant, *Radiat. Eff.* **3,** 249 (1970).
32. R. H. J. Fastenau, A. van Veen, P. Penning and L. M. Caspers, *Physica status solidi* (a) **47,** 577 (1978).
33. J. E. Inglesfield and J. B. Pendry, *Phil. Mag.* **34,** 205 (1976).
34. D. L. Johnson and J. R. Cost, in *Defects and Defect Clusters in B.C.C. Metals and their Alloys, Proc. of National Bureau of Standards Conf.*, Gathersburg, Md, p. 279 (1973).
35. G. R. Odette, P. J. Maziasz and J. A. Spitznagel, *ibid.*, Ref. [13], p. 1289.
36. D. B. Poker and J. M. Williams, *Appl. Phys. Lett.* **40,** 851 (1982).
37. J. Roth, S. T. Picraux, W. Eckstein, J. Bottiger and R. Behrisch, *J. Nucl. Mater.* **63,** 120 (1976).
38. W. Schilling, *Yamada V Conf. on Point Defects*, Tokyo, Japan (1981).
39. F. A. Smidt Jr and A. G. Pieper, in *Properties of Reactor Structural Alloys After Neutron or Particle Irradiation, Proc., of A.S.T.M. Conf.* Gatlinburg, Tenn., p. 352. ASTM-STP-570 (1974).
40. W. D. Wilson and C. L. Bisson, *Radiat. Eff.* **22,** 63 (1974).
41. N. M. Ghoniem, J. N. Al-Hajji and D. Kaletta, *J. Nucl. Mater*, **136,** 192 (1985).
42. A. Evans, *Acta metall.* **28,** 1155 (1980).
43. B. F. Dyson, M. S. Loveday and M. J. Rodgers, *Proc. R. Soc. Ser. A* **349,** 245 (1976).
44. M. Kikuchi, K. Shiozawa and J. R. Weertman, *Acta metall.* **29,** 1747 (1981).
45. J. N. Goodier, *J. appl. Mech.* **55,** 39 (1933).
46. N. J. Grant and A. W. Mullendore (editors) *Deformation and Fracture at Elevated Temperatures.* M.I.T. Press, Cambridge, Mass. (1965).
47. A. F. Smith and G. B Gibbs, *Metals Sci. J.* **2,** 47 (1968).

APPENDIX

Nomenclature

Symbol	*Description*	*Units*
a	lattice constant	m
b	radiation re-solution parameter	
$\dot{C}$	stress controlled nucleation rate	(m^{-2}/s)
C_b^{gb}	grain boundary bubble concentration	(at./at.)
C_g^{gb}	grain boundary single helium atom concentration	(at./at.)
C_{2g}^{gb}	grain boundary di-helium complex concentration	(at./at.)
C_{max}	grain boundary precipitate density	(m^{-2})
D_{gb}	grain boundary self-diffusion coefficient	(m^2/s)
D_v	vacancy self-diffusion coefficient	(m^2/s)
d	grain diameter	(m)
E_{He}^{gb}	effective grain boundary helium migration energy	(eV)
F_v	cavity volumetric shape factor	
G	shear modulus	(MPa)
k	Boltzmann's constant	(eV/K)
K	displacement damage rate	(at./at./s)
L	inter-precipitate spacing	(m)
m_b^{gb}	average number of gas atoms in a bubble	
P	precipitate diameter	(m)
Q_{gb}	grain boundary helium flux	(at./at./s)
$R_{g,b}^{gb}$	reaction rate between single helium and bubbles	(1/s)
$R_{g,g}^{gb}$	reaction rate between two single helium atoms	(1/s)
$R_{g,2g}^{gb}$	reaction rate between single and di-helium clusters	(1/s)
T	temperature	(K)
t	time	(s)
x	distance measured from singularity tip	(m)
α	helium atom impingement frequency	(1/s)
γ_s	cavity surface energy	(J/m^2)
ΔG_c	critical free energy for cavity formation	(eV)

δ	gas re-solution frequency	(1/s)
Δ	effective width of the grain boundary	(m)
ϵ_{GB}	diffusion-controlled combinatorial factor for bubbles	(1/s)
η	grain boundary viscosity	(eV/m^3/s)
λ_{TPJ}	order of stress singularity at triple-point junctions	
ν	Poisson's ratio	
ν_g	helium vibration frequency	(1/s)
σ_L	local stress	(MPa)
σ_P	accentuated stress at the particle face	(MPa)
σ_∞	applied stress	(MPa)
τ_L	characteristic loading time	(s)
τ_R	characteristic relaxation time	(s)